ACS SENSORS

pubs.acs.org/acssensors Article

Rapid Self-Healing Hydrogel with Ultralow Electrical Hysteresis for Wearable Sensing

Seokkyoon Hong, Taewoong Park, Junsang Lee, Yuhyun Ji, Julia Walsh, Tianhao Yu, Jae Young Park, Jongcheon Lim, Claudia Benito Alston, Luis Solorio, Hyowon Lee, Young L. Kim, Dong Rip Kim, and Chi Hwan Lee*

Cite This: https://doi.org/10.1021/acssensors.3c01835 Read Online

ACCESS | Metrics & More | Article Recommendations | Supporting Information

ABSTRACT: Self-healing hydrogels are in high demand for wearable sensing applications due to their remarkable deformability, high ionic and electrical conductivity, self-adhesiveness to human skin, as well as resilience to both mechanical and electrical damage. However, these hydrogels face challenges such as delayed healing times and unavoidable electrical hysteresis, which limit their practical effectiveness. Here, we introduce a self-healing hydrogel that exhibits exceptionally rapid healing with a recovery time of less than 0.12 s and an ultralow electrical hysteresis of less than 0.64% under cyclic strains of up to 500%. This hydrogel strikes an ideal balance, without notable trade-offs, between properties such as softness, deformability, ionic and electrical conductivity, self-adhesiveness, response and recovery times, durability, overshoot behavior, and resistance to nonaxial deformations such as twisting, bending, and pressing. Owing to this unique combination of features, the hydrogel is highly suitable for long-term, durable use in wearable sensing applications, including monitoring body movements and electrophysiological activities on the skin.

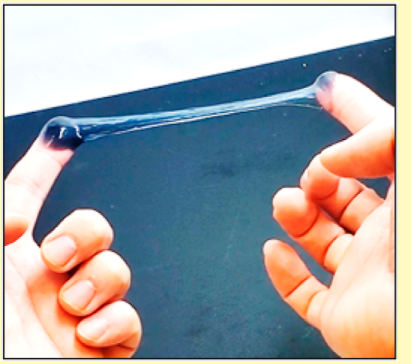

KEYWORDS: *self-healing hydrogels, intermolecular interactions, wearable sensors, strain gauges, electronic skin*

Self-healing hydrogels represent a promising class of materials with the remarkable ability to autonomously repair both mechanical and electrical damages, making them suitable for long-term and durable use in wearable sensing applications.[1−13] This self-healing capability, when incorporated into sensors, can greatly improve their durability and lifespan, protecting them against wear and tear caused by harsh environmental conditions or user misuse.[14−23] These hydrogels are commonly formulated using either dynamic covalent interactions (e.g., borate-esters, disulfide bonds, and imine bonds) or noncovalent interactions (e.g., hydrogen bonds and ionic bonds), which can be easily disrupted and restored.[24−30] Specifically, recent studies have introduced self-healing hydrogels based on poly(vinyl alcohol)−borax hydrogel system.[31,32] Despite their potential benefits, these hydrogels face certain challenges that can reduce their practical effectiveness. For instance, their healing process may be delayed due to a lack of sufficient healing sites.[28,33−35] In addition, they may exhibit substantial electrical hysteresis due to the irreversible energy dissipation of viscoelastic elastomers.[36−39]

Here, we introduce a self-healing hydrogel that exhibits exceptionally rapid healing with a recovery time of less than 0.12 s and an ultralow electrical hysteresis of less than 0.64% under cyclic strains of up to 500%, which originates from the small molecule glycerol with multiple hydroxyl groups. This hydrogel consists of a dynamic and largely interconnected network of poly(3,4-ethylenedioxythiophene)/polystyrenesulfonate (PEDOT/PSS), poly(vinyl alcohol) (PVA), borax, and glycerol. This network structure provides a wealth of intermolecular interactions or healing sites, in comparison to that of other self-healing hydrogels, which leads to shorter recovery times and lower electrical hysteresis (Table S1).[31,40−47] The hydrogel is exceptionally soft with its mechanical modulus (E) of <5.2 kPa, highly deformable with ability to stretch over 10,000%, and also easily reshapable into various shapes that can adapt to intricate contours. Furthermore, it has high ionic and electrical conductivity of >0.074 S m^{-1} and exhibits self-adhesion to the skin with its strength of >0.1 N cm^{-2}. This study involves a systematic investigation of the structure−property−performance relationship of the hydrogel and comparison to its state-of-the-art counterparts. Proof-of-concept demonstrations of the hydrogel include wearable strain gauges in detecting facial expressions, joint bending, and skin deformation from different body parts.

Received: September 1, 2023
Revised: January 8, 2024
Accepted: January 15, 2024

Furthermore, the hydrogel can also function as an electronic skin (e-skin) that can control smartphones and accurately monitor electrophysiological signals such as electrocardiogram (ECG), electromyogram (EMG), and electrooculogram (EOG) directly on the skin, without the need for a conductive ion gel.

RESULTS AND DISCUSSION

Basic Structure and Synthesis Method. Figure 1a includes both a photograph and a schematic illustration of

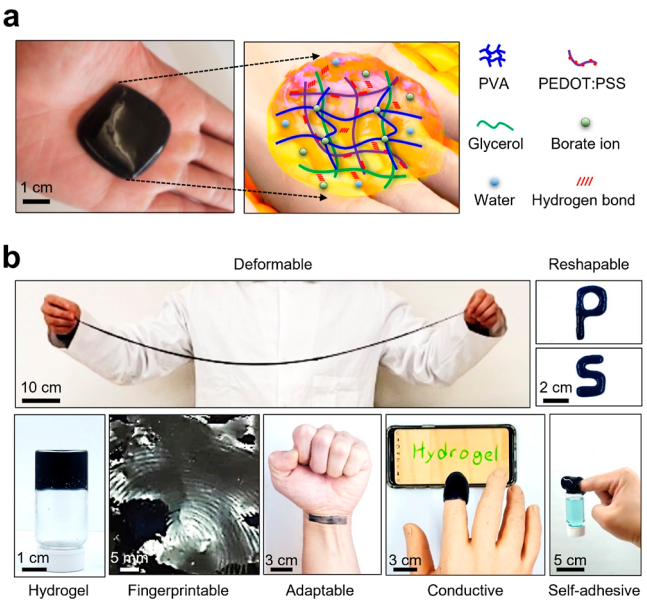

Figure 1. Basic structure and synthesis method. (a) Photograph and schematic illustration of the hydrogel and constituent components. (b) Photographs of the hydrogel, highlighting its remarkable features such as deformability, reshapability, gelation, fingerprintability, adaptability, conductivity, and self-adhesiveness.

the self-healing hydrogel, which is made up of a dynamic and highly interconnected network of PEDOT/PSS, PVA−borax, and glycerol. Glycerol and PEDOT/PSS are blended with PVA−borax hydrogels to create a complex network of intermolecular interactions. When considering the high ratio of hydroxyl groups to its size, small molecule glycerol, with its multiple hydroxyl (−OH) groups, efficiently reacts with borax to form glycerol−borax and glycerol−water networks through hydrogen bonding with water. Meanwhile, the sulfonate groups of PEDOT/PSS can also create hydrogen bonds with borate to form the PEDOT/PSS−borax network. Moreover, the −OH groups on PVA can form hydrogen bonds with both the −OH groups of glycerol and the sulfonate groups on PEDOT/PSS, which generates PEDOT/PSS−PVA and glycerol−PVA networks. This weakening of the PVA−borax cross-linked network leads to greater rearrangement of PVA chains during gelation, increasing its deformability. As a result, the hydrogel exhibited remarkable stretchability, capable of extending to 10,000% of its original length (Figure S1). The synthesis of this hydrogel began by dissolving 1 g of PVA in 9 mL of deionized (DI) water at a temperature exceeding 95 °C for more than 2 h to obtain a PVA solution. Next, 1 g of PEDOT/PSS was added to the PVA solution and stirred for over 2 h until a homogeneous solution was formed. Subsequently, 2 g of glycerol was added to the solution and vigorously stirred over 500 rpm for over 2 h. Meanwhile, 0.4 g of sodium tetraborate was dissolved in 10 mL of DI water until a homogeneous solution was formed. Finally, the hydrogel was formed by stirring the borax aqueous solution and the PVA−PEDOT/PSS−glycerol solution in a 1:4 volume ratio over 500 rpm, which is further confirmed by tube inversion test (Figure S2).[48] The control group was synthesized by the same procedure, excluding glycerol.

Figure 1b showcases photographs of the hydrogel, measuring 2.5 × 2.5 × 0.5 cm^3, highlighting its remarkable features, including (1) exceptional softness, with E < 5.2 kPa, which is 4 times lower than that of control group (Figure S3a); (2) deformability, with the ability to stretch beyond 10,000%; (3) reshaping compliance to mold into various shapes, such as the letters "P" and "S"; (4) complete gelation, (5) distinct fingerprint patterns; (6) adaptability to conform to the intricate contours of uneven surfaces, such as the wrinkles on the wrist; (7) high ionic and electrical conductivity (>0.074 S m^{-1}), allowing it to function as an e-skin capable of manipulating smartphones; and (8) self-adhesion to different surfaces, including plastic (0.35 ± 0.08 N cm^{-2}), glass (0.18 ± 0.002 N cm^{-2}), wood (0.17 ± 0.01 N cm^{-2}), and pigskin (0.10 ± 0.005 N cm^{-2}), which is higher than that of control group (Figure S3b). The self-adhesion of the hydrogel is primarily due to the formation of hydrogen bonds between the hydrogel and substrate, resulting from the abundance of −OH groups in glycerol while the control group has a lower adhesion due to PVA−borax cross-linking, leading to the reduced number of hydroxyl groups for hydrogen bonds (Figure S3c). The hydrogel was also observed to be self-adhesive to human skin, while simultaneously adapting to the movements of fingers and joints (Figure S3d). Real-time demonstrations showcasing these features are shown in Movie S1.

Material Characterization. To gain a comprehensive understanding of glycerol's role within the hydrogel, a control group comprising PVA, borax, and PEDOT/PSS was synthesized. Figure 2a shows scanning electron microscopy (SEM) images of both the control group and the hydrogel, revealing the influence of glycerol on pore size. An intriguing observation emerged with the introduction of glycerol into the control group, resulting in a noticeable reduction in pore size. This phenomenon can be attributed to glycerol's exceptional hydrogen bonding capabilities and its plasticizing effect, which impedes the formation of ice crystals and enhances the flexibility of the hydrogel.[49] As a result, the PVA polymer chains adopt a closer arrangement, ultimately leading to a denser structural configuration.[50] The swelling ratio of the control group and hydrogel was measured to investigate the influence of glycerol on the structure of hydrogels, and the results are shown in Figure 2b. Remarkably, the swelling ratio of the control group surpassed that of the hydrogel samples. This contrast can be directly linked to the inclusion of glycerol, which induced a denser structural arrangement within the hydrogel as shown in Figure 2a. This heightened structural density presented a substantial barrier to water infiltration, resulting in a reduced swelling ratio, declining from 330% for the control group to 112% for the hydrogel. This finding provides compelling support for the concept that the presence of glycerol plays a pivotal role in fostering the formation of additional hydrogen bonds within the hydrogel structure. Fourier transform infrared (FTIR) spectroscopy measurements were conducted to gain insights into the distinctive features of the hydrogels and unravel intermolecular interactions (Figure

https://doi.org/10.1021/acssensors.3c01835
ACS Sens. XXXX, XXX, XXX−XXX

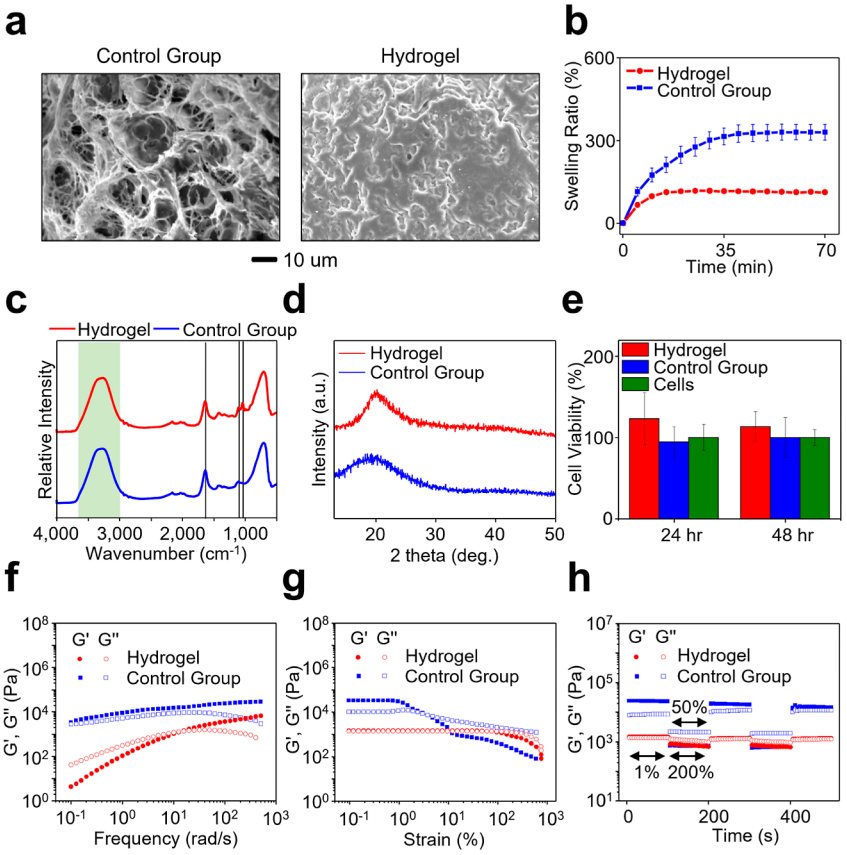

Figure 2. Material characterization. (a) SEM images of the hydrogel and control group. (b) Swelling ratio of the hydrogel and control group. (c) FTIR analysis of the hydrogel and control group. (d) XRD analysis of the hydrogel and control group. (e) Cell viability assay of HPAEC seeded on the hydrogels without (blue bars) and with (red bars) the presence of the glycerol as compared to its bare cells (green bars) (n = 18) using NR assay. (f) G' and G'' of the hydrogel and control group in relation to angular frequency. (g) G' and G'' of the hydrogel and control group in relation to strain. (h) G' and G'' of the hydrogel and control group when alternate step strain switched from small to large strain.

2c). The hydrogels displayed a prominent peak at 1660 cm^{-1}, corresponding to the C═O stretching vibration, a characteristic of the boric ester bond.[51] Another noteworthy absorption peak, around 1106 cm^{-1}, can be attributed to the stretching vibrations of benzenesulfonate.[52] In the range of 3000−3700 cm^{-1}, a broad and intense peak was observed, indicative of symmetrical stretching vibrations of −OH groups, a clear indication of hydrogen bonding.[40] The influence of glycerol on the hydrogel structure was further evidenced by the appearance of additional peaks at 1043 cm^{-1} (Figure S4).[53] It is important to highlight that PVA contains relatively few primary alcohol groups, whereas glycerol primarily consists of primary alcohols.[49] The observed shifts in the C−C−O peak, characteristic of primary alcohols, provide a means to track the hydrogen bonding within the hydrogel. In particular, the control group exhibited a shoulder peak at 1054 cm^{-1}, while the hydrogel displayed a more prominent peak at 1043 cm^{-1}. This shift to lower wavenumbers implies a blue shift in the characteristic absorption spectrum and signifies the formation of stronger hydrogen bonds between PVA and glycerol.[54] This result suggests a substantial interaction between the primary alcohol groups in glycerol and the alcohol groups in PVA, thereby reinforcing intermolecular interactions.[49] Figure 2d shows the X-ray diffraction (XRD) patterns of the hydrogel and the control group. Notably, differences emerged in the full width at half maximum (fwhm) of the peaks after the introduction of glycerol. The reduction in fwhm upon glycerol addition suggests an expansion of the crystalline domains within the hydrogel. This change can be attributed to its role in reinforcing hydrogen bonding networks within the PVA framework. In the case of hydrogel, the structural integrity primarily relies on hydrogen bonding facilitated by its multiple hydroxyl groups interacting with PVA, leading to reduced stability and the formation of larger crystalline domains. In contrast, the control group experiences disruption in the hydrogen bonding network due to the complexation of borate and hydroxyl groups, resulting in smaller crystalline domains and an increased fwhm.[51] This observation underscores its active involvement in enhancing hydrogen bonding interactions within the PVA structure. The time-dependent cell viability of the hydrogels to human pulmonary arterial endothelial cells (HPAECs) was assessed to identify any adverse response at the cellular level (Figure 2e). Specifically, HPAECs were cultured in a vascular cell basal medium with a vascular endothelial growth factor (VEGF) growth supplement (ATCC, PCS-100-041) at 37.5 °C for 24−48 h. The cells were seeded on the surface of the hydrogels and measured using 3-(4,5-dimethylthiazol-2-yl)-2,5-diphenyltetrazolium bromide (MTT) and neutral red (NR) assay kits (Abcam, ab211091 and ab234039, respectively). Details of the cell viability are described in the Experimental Section. Figure 2e shows the experimental results obtained from the hydrogels without (blue bars) and with (red bars) the presence of the glycerol as compared to its bare cells (green bars). The cell viability of the hydrogel remained above 95% throughout the assay period without notable differences among the groups using a NR

https://doi.org/10.1021/acssensors.3c01835
ACS Sens. XXXX, XXX, XXX−XXX

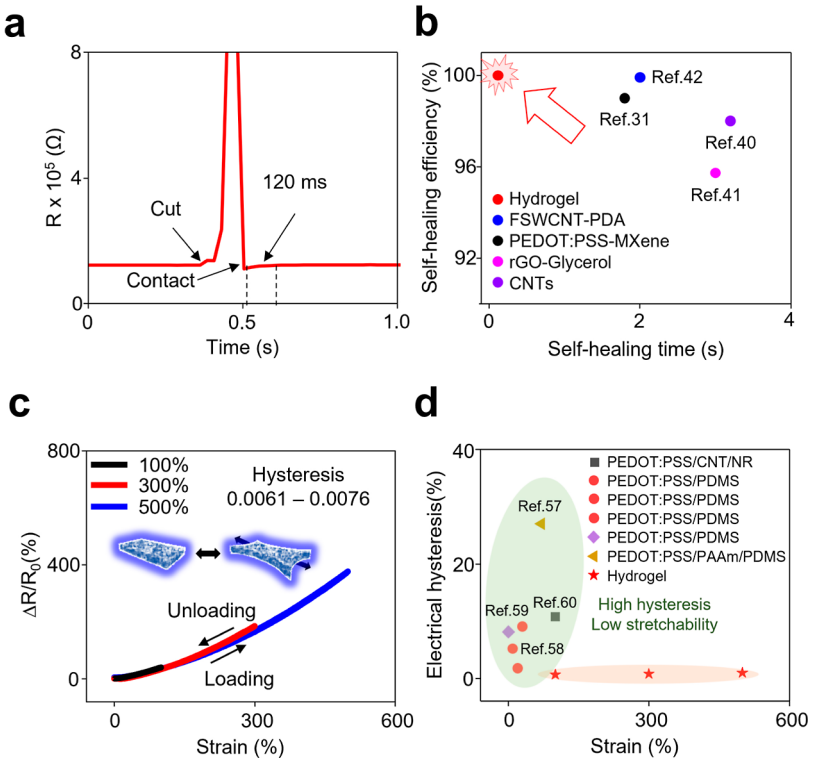

Figure 3. Rapid healing time and ultralow electrical hysteresis. (a) Resistance variation of the hydrogel throughout a cutting and healing process over time. (b) Comparison of self-healing performance with those from prior reports. (c) $\Delta R/R_0$ of the strain gauges under loading−unloading cycles over a wide strain range of up to 500%. (d) Comparison of the electrical hysteresis and strain sensing range of the hydrogel with those from prior reports.

assay (n = 18 for each group). The results closely resemble those obtained from a MTT assay (Figure S5). The results imply that hydrogel would provide safety for potential biomedical applications.

The rheological properties of the hydrogels were characterized by measuring the storage modulus (G') and loss modulus (G'') as a function of angular frequency (Figure 2f). The control group exhibited an elastic behavior, with the storage modulus consistently exceeding the loss modulus across the entire frequency range. The introduction of glycerol at a concentration of 15 wt % resulted in a reduction of both G' and G'', signifying an increased viscosity of the hydrogel due to a reduction of the interaction between PVA and borax.[55] Notably, the hydrogel exhibited distinct rheological behaviors, displaying a viscous response ($G' < G''$) at lower frequencies, below 10 rad/s, and an elastic response ($G' > G''$) at higher frequencies. The sample with a higher glycerol content of 35 wt % displayed the lowest G' and G'' values, with G'' surpassing G', indicating a liquid-like behavior attributed to the plasticizing effect of glycerol (Figure S6a). Consequently, we selected a glycerol content of 15 wt % as the optimal concentration. The behavior of G' and G'' in gel networks can be characterized based on their mode of formation. Covalent bonds yield frequency-independent G' and G'', while non-covalent bonds result in frequency-dependent changes.[56] The G' and G'' of hydrogels displayed frequency-dependent behavior (Figure 2f), suggesting the presence of reversible bonds like hydrogen bonds in the gel network, supported by increasing G' and G'' with frequency.[56] Dynamic rheological testing was utilized to investigate the viscoelastic properties of these hydrogels under a strain sweep (Figure 2g). In the initial phase, the linear viscoelastic region (LVER) of the hydrogels was identified by conducting a strain sweep analysis. Within this range, the G' of the hydrogels remained relatively unaffected by applied strain, indicating the presence of a stable hydrogel structure and G' surpassed G'', in turn indicating elastic gel-like properties (Figure 2g).[56] The LVER extends up to ∼1% strain for the control group and up to a higher strain of ∼80% for the hydrogel. Beyond the LVER, high shear strain began to disrupt the internal network structure of the hydrogel, causing a decline in the storage modulus. Beyond the point where G' crossed G'', the hydrogel displayed yielding behavior, with an increasing collapse of the internal network structure, resulting in a transition from a solid-like state to a liquid-like state. However, the sample with a higher glycerol content of 35 wt % exhibited a higher G'' than G', indicating a liquid-like behavior (Figure S6b). The dynamic cyclic strain sweep tests were conducted to evaluate the mechanical self-healing properties of the hydrogels (Figure 2h). In the low-strain interval, the hydrogel was subjected to constant strain within its LVER where G' exceeded G'', ensuring nondestructive shearing, signifying an elastic gel state. Subsequently, a high-strain interval beyond the LVER was applied, where G' became lower than G'', demonstrating the complete breakdown of the microstructure. Repetitive cycles of low and high strain were employed to evaluate whether the structural deformations caused by high strain can be restored during the low-strain intervals. For instance, at 1% strain, the hydrogel exhibited elastic behavior with G' at 1.48 kPa and G'' at 1.38 kPa ($\tan \delta = G''/G' \approx 0.93 < 1$). At 200% strain, G' and G'' decreased to 0.76 and 1.10 kPa, respectively, displaying viscosity-like behavior ($\tan \delta \approx 1.45 > 1$). Upon reducing the strain amplitude back to 1%, G' and G'' returned to their initial values, indicating rapid network restoration ($\tan \delta \approx 0.94$).

https://doi.org/10.1021/acssensors.3c01835
ACS Sens. XXXX, XXX, XXX−XXX

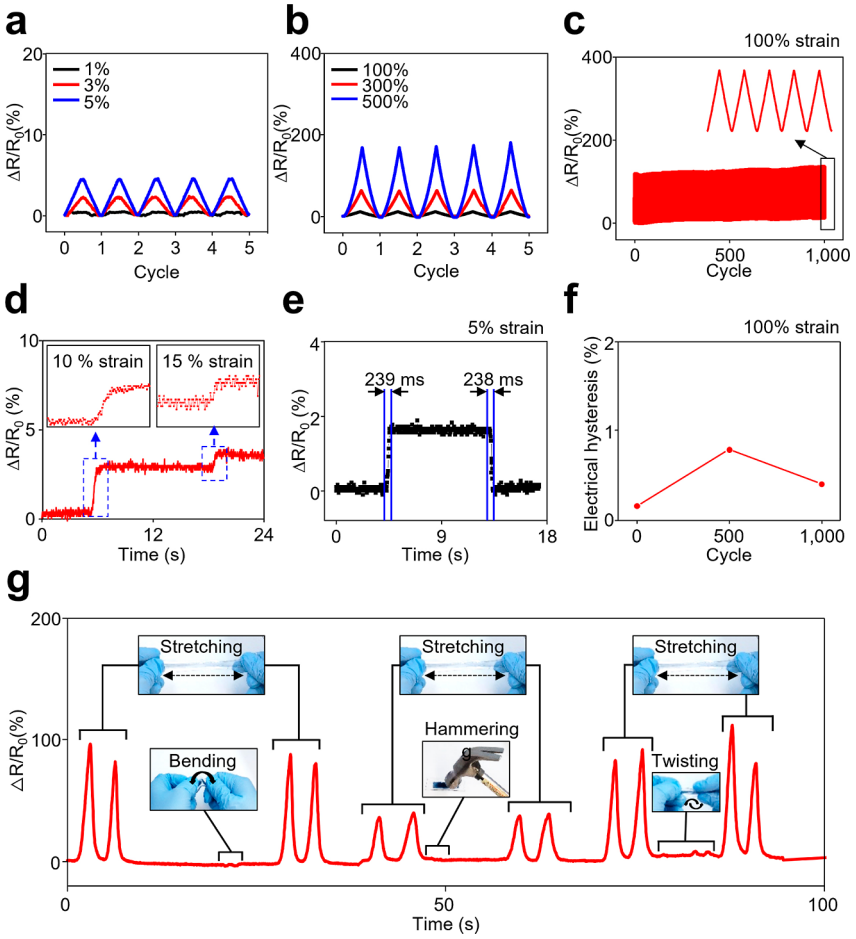

Figure 4. Integration into strain gauges. (a) $\Delta R/R_0$ of the strain gauges under loading−unloading cycles at strains of 1, 3, and 5%. (b) $\Delta R/R_0$ of the strain gauges under loading−unloading cycles at higher strains of 100, 300, and 500%. (c) $\Delta R/R_0$ of the hydrogel throughout 1000 cycles of stretching at a strain of 100%. (d) $\Delta R/R_0$ versus time for step-strain characterizations. (e) Response/recovery time of the hydrogel. (f) Electrical hysteresis of the hydrogel. (g) Selective response of the hydrogel to stretching compared to other deformation modes, with insets showcasing its behavior under stretching, bending, hammering, and twisting.

The control group also demonstrated the self-healing properties. However, self-healing behavior cannot be observed in the sample with a high glycerol content of 35 wt % due to its primarily liquid-like behavior (Figure S6c). To further assess the mechanical self-healing properties of the hydrogels, "cut and stick" experiments were conducted. The hydrogel was intentionally severed and promptly reconnected, and its capability to undergo elongation was demonstrated (Figure S7).

Rapid Healing Time and Ultralow Electrical Hysteresis. In wearable sensing applications, low electrical hysteresis is crucial for ensuring consistent, easily interpretable data in human motion detection, thus simplifying calibration and enhancing reliability in comparative analysis.[7,36,38] Figure 3a presents the resistance variations of the hydrogel throughout the cutting and healing process over time. Upon being fully cut into two pieces, the resistance of the hydrogel increased to infinity, but it resumed to its initial value after only 0.12 s of the healing process. Consequently, the hydrogel demonstrated the fastest recovery time (0.12 s) and the highest self-healing efficiency (~100%), compared to those of other self-healing hydrogels (Figure 3b).[31,40−42] The self-healing time is also 35 times faster than that of the control group (4.2 s) (Figure S8a). The outstanding self-healing ability of the hydrogel is primarily due to the small molecule glycerol, with its multiple hydroxyl groups, which provides many free borax chelating sites for wound self-repair (Figure S8b). Real-time demonstrations of the hydrogel connected in series with a light-emitting diode (LED), which turns off and on during cutting and immediately after a healing process, respectively, are shown in Movie S2. The remarkably rapid healing time can be attributed to a reduction in covalent bonds (i.e., PVA−borax) and an increase in hydrogen bonds (i.e., glycerol−borax, glycerol−PVA, PEDOT/PSS−borax, and PEDOT/PSS−PVA) as covalent bonding takes longer to heal than noncovalent bonding (Figure S9).[1,24]

This unique feature of the hydrogel results in ultralow electrical hysteresis, making it an ideal material for strain gauges. To demonstrate this, the hydrogel was encapsulated with thin layers (<500 μm thick) of acrylic sealer (VHB-4905; 3M Inc.) with conductive films (CST5; Digi-Key, Inc.) inserted as recording electrodes. The manufacturing process of strain gauges commenced with grooves being created in the encapsulation material (Figure S10a). The grooved layer was then bonded to the lower encapsulation layer using adhesive. Subsequently, copper electrodes were positioned at the extremities of the grooved layer, which was filled with hydrogel to ensure robust electrical contact. The assembly was completed by attaching the top encapsulating layer with glue. Its structural representation, along with a corresponding

https://doi.org/10.1021/acssensors.3c01835
ACS Sens. XXXX, XXX, XXX−XXX

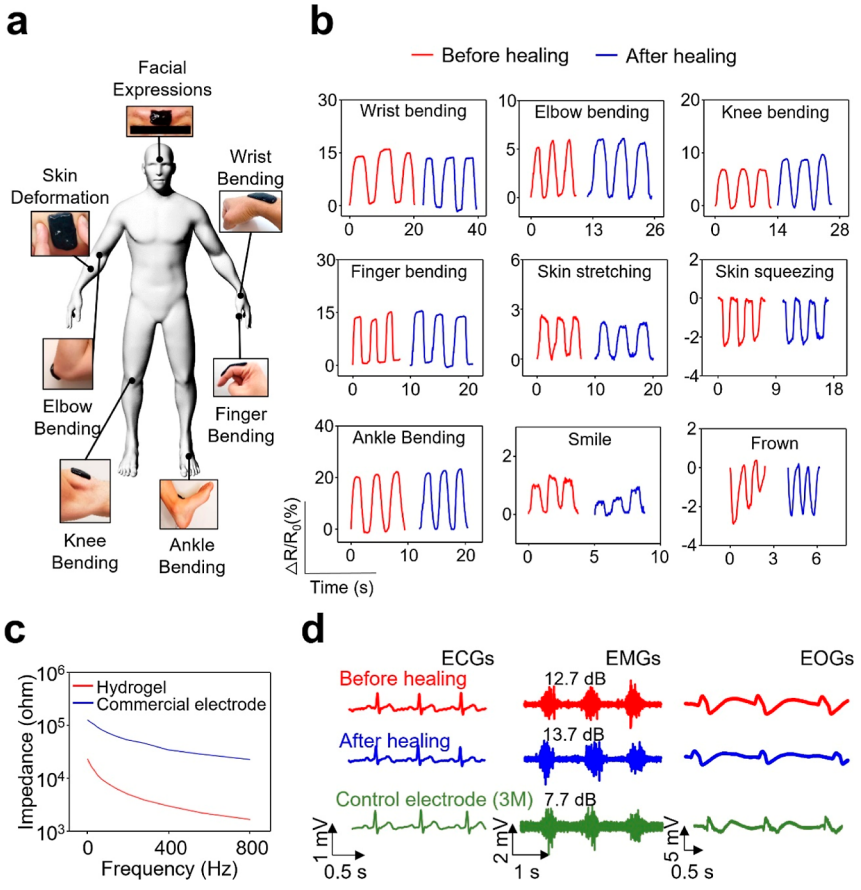

Figure 5. Proof-of-concept demonstrations in wearable sensing applications. (a) Schematic illustration of the sensing location. (b) Strain sensing results from various skin deformations or vibrations on different body parts. (c) Comparison of the electrode–skin contact impedances between the hydrogel (red) and commercial recording electrodes (blue). (d) ECG, EMG, and EOG signals obtained from the forearm and near the eye of a volunteer using the hydrogel versus commercial recording electrodes.

photograph, is shown in Figure S10b. The resulting strain gauges are highly soft (E = 123 kPa), stretchable (up to 860%), compressible, foldable, and twistable (up to 360°) without compromising the inherent properties of the hydrogel, up to the point of rupture of the encapsulation layer at a strain of ~880% (Figure S10c). To further elucidate the mechanical characterization of the strain gauges, the cyclic tensile loading–unloading tests with strains reaching up to 100% were conducted. Mechanical hysteresis was observed and attributed to the viscoelastic properties of the encapsulation layers (Figure S11a). Nevertheless, following the initial cycle, a reduction in hysteresis was observed, indicative of the softening of the encapsulation layers (Figure S11b). However, a strain gauge using the control group has revealed an observable detachment between the copper electrode and the control group when subjected to stretching, primarily attributed to the absence of glycerol, which enhances deformability. This phenomenon imposes constraints on the practical applicability of the strain sensor (Figure S12). Figure 3c presents the relative resistance change ($\Delta R/R_0$) of the strain gauges under loading–unloading cycles over a wide strain range of up to 500%. The results indicate negligible electrical hysteresis, with values of 0.61 ± 0.45, 0.76 ± 0.18, and 0.64 ± 0.58% at strains of 100, 300, and 500%, respectively (n = 3 each). Consequently, the strain gauges exhibited full-scale, ultralow electrical hysteresis across a broad strain range, in contrast to previously reported PEDOT/PSS-based materials that are limited by rigid conducting polymers and irreversible energy dissipation (Figure 3d).[57−60] Importantly, the ultralow electrical hysteresis of the strain gauges remained consistent even after more than a week (Figure S13).

Integration into Strain Gauges. Figure 4a displays the $\Delta R/R_0$ of the strain gauges under loading–unloading cycles at low strains of 1, 3, and 5%. Figure 4b shows the consistent results at high strains of 100, 300, and 500%. These results were consistent with over 1000 cycles of strains beyond 100%, demonstrating the excellent stability and continuous performance of the strain gauges under multiple cycles of both low and high strains (Figure 4c). The $\Delta R/R_0$ of the strain gauges quickly increased when subsequently stretched at strains of 10 and 15% and then remained at a stable level, with no sharp peaks (Figure 4d). The response and recovery times of the hydrogel under a 5% strain with a loading and unloading rate of 500 mm min^{-1} were measured as ~238 ms (Figure 4e). As the strain increased to 10, 100, and 200%, the response and recovery time also increased to approximately 441 ms, 3.1 s, and 6.6 s, respectively (Figure S14). Notably, the strain gauges exhibited negligible overshoot or relaxation behavior unlike others made of elastomers.[61−64]

The strain gauges maintained ultralow electrical hysteresis of <1% against >1000 cycles of stretching at the applied strain of 100% (Figure 4f). The corresponding data for $\Delta R/R_0$ versus strain at the 1st, 500th, and 1000th cycles are shown in Figure S15a. The strain gauge exhibited remarkable stability and low

https://doi.org/10.1021/acssensors.3c01835
ACS Sens. XXXX, XXX, XXX−XXX

drift across 1000 cycles of stretching and releasing, without failure, at an applied strain of up to 200% (Figure S15b). Figure 4g demonstrates that the strain gauges were only sensitive to axial stretching and remained barely changed upon hammering and bending, as evidenced by the barely changed $\Delta R/R_0$ values. Consistently, the $\Delta R/R_0$ of the strain gauges remained unchanged against compression, bending, and twisting (Figure S16). This unique behavior of the hydrogel stems from the resistance of its polymer chains to compression, bending, and twisting, which leads to insufficient forces being exerted on the hydrogen bonds, thereby preventing disruption of the conductive domain (i.e., PEDOT/PSS).[36] Conversely, when the hydrogel is stretched, the distance between the conductive domain increases, leading to a corresponding increase in $\Delta R/R_0$.[65] Real-time demonstrations showcasing these behaviors are shown in Movie S3. The sensitivity of strain gauge can be quantified through the gauge factor (GF). The GF values are with an initial measurement of 0.7 within the strain range of 0−300% (Figure S17). This factor subsequently rises to 1.5 within the range of 300− 600% strain and further improves to 2.3 within the range of 600−866% strain. These GF values, as shown in Figure S17b and Table S2, are notably higher than those reported for recently developed hydrogel sensors.[31,40,46,66,67] This heightened sensitivity underscores its suitability for precise strain sensing applications. Nevertheless, at very low strain levels, such as those associated with subtle skin deformation, a strain gauge using the hydrogel exhibited a relatively low gauge factor, making it suitable for the measurement of electrophysiological signals.

Proof-of-Concept Demonstrations in Wearable Sensing Applications. In the field of wearable sensing applications, the self-healing capability assumes paramount importance as it has a direct impact on the durability, reliability, and lifespan of wearable devices, particularly in instances where damage can occur due to user mishandling.[6,7] To demonstrate the utility of the hydrogel in the context of human motion tracking and electrophysiology monitoring, several testbed specimens were tailored in size and shape. Furthermore, both the initial hydrogel specimens and those that had undergone a healing process were employed to validate the durability under external mechanical damage in the context of wearable applications. To showcase an example of the hydrogel for human motion tracking, the hydrogel was effortlessly attached to various positions on the human body without the need for additional adhesives (Figure 5a). Then, the specimens were designed to measure strain changes ranging from minor (0−5%) to substantial (5−50%) in various body parts, including the facial muscles (i.e., smile and frown), joints during bending (i.e., wrist, elbow, knee, finger, and ankle), skin deformation (i.e., skin stretching and squeezing) of an adult volunteer (32 years old; male) and demonstrated consistent performance in tracking body motions after healing from a complete cut (Figure 5b).

The skin−electrode impedance, a critical factor influencing the quality of recorded biosignals, was assessed using hydrogel electrodes on the skin. In these tests, the hydrogel electrode functioned as the working electrode (WE), while two separate commercial Ag/AgCl electrodes (RedDot, 3M, USA) served as the reference electrode (RE) and counter (CE) electrode, respectively. The phase response of the hydrogel is similar to that of commercial electrodes (Figure S18). The hydrogel exhibited significantly lower impedance compared to that of commercial Ag/AgCl electrodes, as shown in Figure 5c. This lower impedance is primarily attributed to its softness ($E < 5.2$ kPa), enabling it to conform closely to the skin's contours and ensure a secure attachment.[68] Notably, the signal-to-noise ratio (SNR) of electromyographic signals acquired using hydrogel electrodes (12.7 dB) was higher than those obtained with the commercial 3M Ag/AgCl electrode (7.7 dB), which supports the suitability of hydrogel-based electrodes for EMG signal recording. The SNR of EMG signals (13.7 dB) from hydrogels remains consistent even after the healing process, which emphasizes the stability of hydrogels after the healing process (Figure 5d). Figure 5d presents the comparison of electrophysiological signal measurements, including ECG, EMG, and EOG, obtained from the forearm and near the eye of the volunteer using the hydrogel versus commercial recording electrodes (RedDotTM, 3M, USA). The captured ECG, EMG, and EOG signals effectively displayed the P, Q, R, S, and T waves of cardiac activity, neuromuscular activities, and eye movements.[69,70] There were no significant quantitative differences between the measurements taken with the hydrogel electrodes before and after the healing process. Real-time demonstrations showcasing these applications are shown in Movie S4.

Importantly, no signs of skin irritation were observed during these demonstrations. To further confirm, skin irritation tests were confirmed, as detailed in the Experimental Section. The hydrogel and 3M tapes were applied to human skin for approximately 10 min and then removed. A control group consisted of bare skin without any treatment. Figure S19 presents the results, which show no significant difference in irritation between the hydrogel and the control group ($p = 0.81454$). However, significant differences were found between the 3M tape and the control group ($p = 0.00609$), as well as between the 3M tape and the hydrogel ($p = 0.02682$). The hydrogel caused no notable skin irritation, and the volunteer experienced no pain during removal. In contrast, the 3M tapes induced skin irritation, particularly upon removal. These findings underscore the excellent biocompatibility of the hydrogel, which can be attributed to its composition of entirely biocompatible materials, including PVA−borax, PEDOT/PSS, and glycerol.

CONCLUSIONS

This study introduces an unprecedentedly rapid self-healing hydrogel, with a healing time of under 0.12 s and ultralow electrical hysteresis of less than 0.64% during cyclic stretching at high strains of up to 500%. The hydrogel boasts a multitude of desirable properties, including exceptional softness, deformability, adaptability to complex surfaces, reshapability, and self-adhesion to the human skin. A harmonious balance is achieved between its cyclic and step-strain sensing capabilities, response and recovery times, absence of overshoot behavior, durability, and resistance to off-axial deformation, without any compromises. The unique characteristics of the hydrogel can be ascribed to its distinct network structure, formed through robust interconnections and dynamic interactions among its constituents. Wearable sensors fabricated from this hydrogel deliver dependable performance in tracking human motion and electrophysiological monitoring, even after recovering from a full severance. The hydrogel offers immense potential for wearable sensing applications, paving the way for advancements in various fields such as sports medicine, prosthetics, and robotics.

https://doi.org/10.1021/acssensors.3c01835
ACS Sens. XXXX, XXX, XXX−XXX

EXPERIMENTAL SECTION

Materials. PVA (M_w: 146,000−186,000), PEDOT/PSS, glycerol, and sodium tetraborate were purchased from Sigma-Aldrich, and the encapsulating tape (VHB 4905) was purchased from 3M. All reagents were used as-received without further purification, and the Cu tapes (CST5) were purchased from Digi-Key.

Hydrogel Synthesis. A total of 9 g of DI water was added to 1 g of PVA and stirred at 95 °C until completely dissolved. The PVA solution was then thoroughly stirred together with 1 g of PEDOT/PSS solution for over 2 h. Subsequently, 2 g of glycerol was added to the PVA−PEDOT/PSS solution, which was further stirred for over 2 h until a homogeneous solution was obtained. In the meantime, 0.4 g of sodium tetraborate was dissolved in 10 mL of deionized water to form a homogeneous solution. Finally, the borax aqueous solution was mixed with the PVA−PEDOT/PSS−GL solution in a 1:4 volumetric ratio by stirring to obtain the PVA−PEDOT/PSS−GL hydrogel. The PVA−PEDOT/PSS hydrogel for the control group was synthesized using the same procedure as described above, excluding the glycerol. The borax aqueous solution and PVA−PEDOT/PSS−GL solution mixed in a 1:4 volumetric ratio and ∼8 wt % PVA solution were used for synthesizing highly cross-linked hydrogels to emphasize the glycerol's plasticizing effect.[71,72]

Structural Analysis. The hydrogels underwent a 48 h lyophilization process with a Scientific Pro Freeze-Dryer (HR7000-M; Harvestright, LLC.). Subsequently, their structural intricacies were examined using a high-resolution scanning electron microscope (S-4800; Hitachi, Inc.).

FTIR Spectroscopy. FTIR spectroscopy (Thermo Nicolet 6700) was performed in absorption mode with a scan range of 500−4000 cm^{-1}, 36 scan acquisitions, and a resolution of 4 cm^{-1}. The hydrogels were placed on the measuring area that covers the whole surface of the FTIR crystal.

XRD Analysis. XRD spectra were obtained using an X-ray diffractometer (PANalytical X'pert Pro) at 45 kV and 40 mV.

Swelling Ratio. Swelling properties of the hydrogels were studied by measuring their weight change during the uptake of water. The hydrogels were freeze-dried to a constant weight and then immersed in DI water at 25 °C until their weight became stable. In order to determine the weight changes of the hydrogel at different time intervals, the hydrogel was weighed every 5 min with any excess surface moisture removed with filter paper prior to weighing. The swelling ratio of sample was calculated according to the following eq 1

$$\text{swelling ratio } (\%) = \frac{W_1 - W_2}{W_1} \times 100\% \tag{1}$$

where W_1 is the sample weight in swollen-saturated state and W_2 is the sample weight in dry state.

Cell Viability. The samples were placed into a 24-well plate. HPAECs were seeded inside the wells with a density of 2×10^5 per well in vascular cell basal medium with an VEGF growth kit (ATCC, PCS-100-041) and then incubated at 37.5 °C with 5% carbon dioxide (CO_2) for 48 h. At each 24 h, MTT (Abcam, ab211091) and NR (Abcam, ab234039) assays were carried out according to each kit's protocols. The absorbance was then measured using a microplate reader (Synergy H1, BioTek) at wavelengths of 590 and 540 nm, respectively.

Rheology. A rheometer (Discovery HR-2; TA Instruments, Ltd.) was used to measure the rheological properties of the hydrogels using parallel-plate geometry (20 mm diameter) with a gap of 950−1050 μm. The LVERs of the samples were determined through amplitude sweep measurements, wherein the strain % was varied in the range of 0.1−500 at a constant frequency of 15 rad/s. Frequency sweep measurements were conducted within the angular frequency range of 0.1−500 rad/s, maintaining a constant strain well within the LVER. To assess the mechanical self-healing properties of the hydrogels, the continuous cycles of low-strain oscillatory shear (1%) for a duration of 100 s within the LVER, followed by high-strain conditions for a duration of 100 s beyond the LVER were conducted (50 or 200% for the control group or hydrogels, respectively). These tests were performed at a constant angular frequency of 15 rad/s. The samples were carefully weighed and loaded onto the stationary bottom plate. Subsequently, the top plate was lowered automatically at a controlled rate to ensure a reproducible gap height and complete filling of the sample between the plates before measurement.

Integration into Strain Gauges. Two encapsulating tapes sandwiched the hydrogel. Before encapsulation, encapsulating tape was used to form a groove, and the grooved layer was attached to another encapsulating tape with glue. Next, two copper electrodes were fixed at the ends of the encapsulating tape, which was then filled with the hydrogel to establish good contact with the two copper electrodes. The strain sensor was completed by attaching another encapsulating tape on top with glue. This enabled the hydrogel to be encapsulated in rectangular-shaped grooves.

Electrical and Adhesion Characterizations. The resistance of the hydrogel was measured in a two-wire configuration using a source meter (Keithley 2400; Tektronix, Inc.). A two-wire configuration was employed for its appropriateness in measuring resistance values ranging above 100 Ω. The electrical conductivity of the hydrogel was calculated as following eq 2

$$\sigma = \frac{1t}{RA} \tag{2}$$

where R is the measured resistance, t is the sample thickness, and A is the sample area. The values for A, t, and R are as follows: A = 0.00005 m^2, t = 0.0005 m, and R = 70,600, 59,800, and 74,000 Ω. Adhesion measurements were conducted between the hydrogels and substrates in a perpendicular geometry. An indenter with a diameter of 12 mm was used to cast the hydrogel, which was attached to the load cell, brought into contact with the substrate for around 10 s, and then successively pulled off. The maximum force normalized to the area of substrate covered by the hydrogel was calculated as the adhesion force.

Self-Healing Characterization. A glass slide was used to place a hydrogel, measuring 4 × 4 × 0.5 cm^3, which was then cut using a razor blade. Electrical self-healing experiments were performed on the hydrogel samples. Silicone cover stranded-core wires (DYR-46202, Adafruit) were positioned at the bottom ends of the hydrogel, and the resistance of the hydrogel was measured in a two-wire configuration using a source meter (Keithley 2400; Tektronix, Inc.). The electrical healing efficiency was calculated using the following eq 3

$$\eta = \frac{R_r}{R_i} \tag{3}$$

where R_r is the recovered conductivity and R_i is the initial conductivity.

Electrical and Mechanical Hysteresis Characterization. The electrical hysteresis of the strain sensor was assessed by setting the resistance of each cycle as the initial value when plotting the curves of $\Delta R/R_0$ versus strain. The width of the hysteresis loop was used to determine the degree of hysteresis. The areal variation between the loading and unloading states of relative electrical signal change versus strain was defined quantitatively as electrical hysteresis using the following eq 4

$$H = \frac{|A_L - A_U|}{A_U} \times 100\% \tag{4}$$

where A_L and A_U are the areas of relative electrical signal change versus strain in the loading and unloading states, respectively. Mechanical hysteresis (H_M) was defined as the areal difference under stress−strain curves during loading−unloading cycles and computed by the following eq 5

$$H_M = \frac{|A_L - A_U|}{A_U} \times 100\% \tag{5}$$

where A_L and A_U are the area under the stress−strain graph in loading and unloading states, respectively (Figure S20).

Gauge Factor. GF is defined by the following eq 6

https://doi.org/10.1021/acssensors.3c01835
ACS Sens. XXXX, XXX, XXX−XXX

$$GF = (\Delta R/R_0)/\varepsilon \quad (6)$$

where R_0, ΔR, and ε are the initial resistance before stretching, difference of resistance under stretching, and applied strain, respectively. The GF of the hydrogel was obtained from a linear fitting divided by three linear regions.

Human Motion Detection. Silicone cover stranded-core wires (Adafruit, Inc.) were attached to both sides of the hydrogel to serve as electrical connectors, after which the hydrogel was mounted on the skin of various body parts. In the process of measuring, the wires were connected to a source meter (Keithley 2400; Tektronix, Inc.) in a two-wire configuration.

Impedance Spectroscopy. Impedance assessment was conducted using a potentiostat (SP-200, BioLogic) in a three-electrode setup, with the electrodes spaced 4.0 cm apart, center-to-center. For comparative purposes, a commercial Ag/AgCl electrode was used as the WE in evaluations against the hydrogel. The surface area of both the commercial Ag/AgCl electrode and the hydrogel was 3.24 cm^2. All tests were performed on the forearm, using potentiometric mode, and applying a sinusoidal signal with a 1 mV amplitude. The frequency range for the measurements spanned from 1 to 800 Hz.[73]

SNR Calculation. The SNR was calculated using power spectral density estimation in MATLAB. The SNR in decibels (dB) was calculated using the following formula 7

$$SNR_{dB} = 10 \log_{10}\left(\frac{P_{signal}}{P_{noise}}\right) \quad (7)$$

where P_{signal} is power of signal and P_{noise} is power of noise.

Electrophysiological Recording. The conductive hydrogels were attached to the forearm and near the eye of a volunteer to measure ECG, EMG, and EOG signals. The signals were transmitted remotely to an external computing system by connecting the hydrogels to a portable wireless unit (BioRadioTM, Great Lakes NeuroTechnologies, Cleveland, OH, USA). The type of filter is a notch filter, used to reduce interference from the 60 Hz electrical powerline frequency and its harmonics, ensuring accurate recording of biological signals. The commercial software (BioCapture, Great Lakes NeuroTechnologies, USA) was employed, with filtering at 60 Hz. The filtered data were subsequently exported remotely to MATLAB for data postprocessing. The suitability of hydrogel for electrophysiological signal recording hinges on its ability to consistently maintain a stable electrical connection with the skin rather than the sensitivity to mechanical strains.

Skin Irritation Testing. Hyperspectral line-scan images (hypercube) of human skin were obtained to study inflammation, which is commonly characterized by erythema and changes in hemoglobin concentrations, following skin irritation.[74,75] A monochrome camera (GS3-U3-120S6M-C; FLIR) with a slit width of 23 μm and groove density of 150 mm^{-1} was used for imaging, and an LED light source with a color temperature of 6500 K (D65) was employed for illumination. Spectral calibration of the spectrograph was performed using a xenon calibration light source that emitted multiple narrow peaks at specific wavelengths. A fixed focal length lens (MVL25M1; Navitar) was primarily used for imaging the skin, with a field of view as small as 10 mm × 10 mm. RGB images were captured with a smartphone camera (iPhone 11 Pro; Apple) of the same area. The hydrogel was applied to the medial antebrachial cutaneous of the forearm for approximately 10 min. A 3M tape was attached to the same area for 10 min as a positive control. Images were taken before and after the experiment to compare hemoglobin content. A mechanical linear scan step was performed at 0.25 mm, and a custom MATLAB interface was used for data acquisition. A tissue reflectance spectral model was applied to extract key hemodynamic parameters from the ground-truth hyperspectral image. The theory of radiative transport and robust approximations (e.g., diffusion, Born, and empirical modeling) were used to model light propagation in tissue, and the intensity reflected from a biological sample can be expressed as a function of λ in the visible range

$$I_R(\lambda) = \left[b_1\left(\frac{\lambda}{\lambda_0}\right)^{b_2} + b_3\left(\frac{\lambda}{\lambda_0}\right)^{-4}\right] \exp[-b_4 \times \{b_5 \times \varepsilon_{HbO_2}(\lambda) + (1 - b_5) \times \varepsilon_{Hb}(\lambda)\}] \quad (8)$$

where b_1, b_2, and b_3 are associated with the scattering (Mie or Rayleigh) contributions at λ_0 = 800 nm, $\varepsilon_{HbO_2}(\lambda)$ denotes the absorption coefficient of oxygenated hemoglobin (HbO_2), $\varepsilon_{Hb}(\lambda)$ denotes the absorption coefficient of deoxygenated hemoglobin (H_b), b_4 is the hemoglobin concentration multiplied by the optical path length, and b_5 is the blood oxygen saturation (sPO_2). In the study, the value of hemoglobin contents multiplied by the optical path length (b_4) was used to indicate the level of skin irritation by eq 8. All fitting parameters were computed using the simplex search (Nelder–Mead) algorithm.

■ ASSOCIATED CONTENT

Supporting Information

The Supporting Information is available free of charge at https://pubs.acs.org/doi/10.1021/acssensors.3c01835.

Manual tensile test of the hydrogel; tube inversion test of the hydrogel; stress–strain curve of the hydrogel and control group, adhesion strength of the hydrogel and control group to various substrates, schematic images illustrating the adhesion mechanisms of the hydrogel and control group to different substrates, photographs of the hydrogel adhering to fingers and joints; FTIR results of the hydrogel and control group; cell viability assay of HPAEC seeded on the hydrogels without (blue bars) and with (red bars) the presence of the glycerol as compared to its bare cells (green bars) using MTT assay (n = 18); G' and G'' of the sample with a glycerol content of 35 wt % in relation to angular frequency, G' and G'' of the sample with a glycerol content of 35 wt % in relation to strain, G' and G'' of the sample with a glycerol content of 35 wt % when alternate step strain switched from small (1%) to large strain (200%); self-healing time comparison between the hydrogel and control group, schematic diagrams illustrating the self-healing sites of the hydrogel and control group; schematic diagrams illustrating the self-healing mechanism of the hydrogel; fabrication process of strain gauges, schematic illustration and photograph of the hydrogel integrated into a strain gauge, stress–strain curve and photograph of the strain gauge under stretching, compression, folding, and twisting; cyclic stress–strain curves of the strain gauges at strains of 100%, mechanical hysteresis of the strain gauges; R/R_0 of the strain gauges using the control group with an inset highlighting a disconnection between the copper electrode and the control group; $\Delta R/R_0$ of the strain gauges under loading–unloading cycles over a wide strain range of up to 500% on day 7, electrical hysteresis of the strain gauges on day 1 and 7; response/recovery time of the strain gauges; $\Delta R/R_0$ of the strain gauges throughout 1000 cycles of stretching with a strain of 100%, highlighting its ultralow electrical hysteresis of <1%, $\Delta R/R_0$ of the hydrogel throughout 1000 cycles of stretching at a strain of 200%; $\Delta R/R_0$ of the hydrogel under compression, bending, and twisting; gauge factor of the strain gauge, comparison diagram of strain sensing properties of the hydrogel with other reported PVA-gel-

https://doi.org/10.1021/acssensors.3c01835
ACS Sens. XXXX, XXX, XXX–XXX

based strain sensor; comparison of the phase response between the hydrogel (red) and commercial recording electrodes (blue); RGB images of the forearm skin before (control) and after application of the hydrogel; comparison of performance between the hydrogel reported in this work and previously reported self-healing hydrogels; schematics of H_E and H_M; comparison of performance between the hydrogel reported in this work and previously reported self-healing hydrogels; and gauge factor comparison between the strain gauge developed here and recently reported hydrogel-based sensors (PDF)

Real-time demonstrations showcasing the key features of the hydrogel including deformability, reshapability, gelation, fingerprintability, adaptability, conductivity, and self-adhesiveness (MP4)

Real-time demonstrations of the hydrogel connected in series with an LED, which turns off and on during cutting and immediately after a healing process (MP4)

Real-time demonstrations exhibiting the selective response of the hydrogel to stretching, compared to that for other types of deformation such as compression, bending, and twisting (MP4)

Real-time demonstrations showcasing the use of the strain gauges for human motion tracking from various body parts (MP4)

AUTHOR INFORMATION

Corresponding Author

Chi Hwan Lee − *Weldon School of Biomedical Engineering, Purdue University, West Lafayette, Indiana 47907, United States; Center for Implantable Devices, School of Mechanical Engineering, and School of Materials Engineering, Purdue University, West Lafayette, Indiana 47907, United States;* orcid.org/0000-0002-4868-7054; Email: lee2270@purdue.edu

Authors

Seokkyoon Hong − *Weldon School of Biomedical Engineering, Purdue University, West Lafayette, Indiana 47907, United States;* orcid.org/0009-0007-6540-0389

Taewoong Park − *Weldon School of Biomedical Engineering, Purdue University, West Lafayette, Indiana 47907, United States*

Junsang Lee − *Weldon School of Biomedical Engineering, Purdue University, West Lafayette, Indiana 47907, United States; School of Mechanical Engineering, Hanyang University, Seoul 04763, Republic of Korea*

Yuhyun Ji − *Weldon School of Biomedical Engineering, Purdue University, West Lafayette, Indiana 47907, United States*

Julia Walsh − *Weldon School of Biomedical Engineering, Purdue University, West Lafayette, Indiana 47907, United States;* orcid.org/0000-0001-6637-7191

Tianhao Yu − *School of Mechanical Engineering, Purdue University, West Lafayette, Indiana 47907, United States;* orcid.org/0000-0001-9637-352X

Jae Young Park − *Weldon School of Biomedical Engineering, Purdue University, West Lafayette, Indiana 47907, United States*

Jongcheon Lim − *Weldon School of Biomedical Engineering, Purdue University, West Lafayette, Indiana 47907, United States*

Claudia Benito Alston − *Weldon School of Biomedical Engineering, Purdue University, West Lafayette, Indiana 47907, United States;* orcid.org/0000-0002-8957-5083

Luis Solorio − *Weldon School of Biomedical Engineering, Purdue University, West Lafayette, Indiana 47907, United States*

Hyowon Lee − *Weldon School of Biomedical Engineering, Purdue University, West Lafayette, Indiana 47907, United States; Center for Implantable Devices, Purdue University, West Lafayette, Indiana 47907, United States;* orcid.org/0000-0001-7628-1441

Young L. Kim − *Weldon School of Biomedical Engineering, Purdue University, West Lafayette, Indiana 47907, United States;* orcid.org/0000-0003-3796-9643

Dong Rip Kim − *School of Mechanical Engineering, Hanyang University, Seoul 04763, Republic of Korea;* orcid.org/0000-0001-6398-9483

Complete contact information is available at: https://pubs.acs.org/10.1021/acssensors.3c01835

Notes

The authors declare the following competing financial interest(s): A patent application related to the self-healing hydrogel has been filed to the U.S. patent office for consideration.

ACKNOWLEDGMENTS

This work is funded by the Eli Lilly and Company. C.H.L. acknowledges the Leslie A. Geddes Endowment at Purdue University. J.L. acknowledges the funding support from the MOTIE (Ministry of Trade, Industry, and Energy) in Korea, under the Human Resource Development Program for Industrial Innovation (Global) (P0017306, Global Human Resource Development for Innovative Design in Robot and Engineering) supervised by the Korea Institute for Advancement of Technology (KIAT).

REFERENCES

(1) Kang, J.; Tok, J. B.-H.; Bao, Z. Self-healing soft electronics. *Nat. Electron.* **2019**, *2*, 144−150.

(2) Son, D.; Kang, J.; Vardoulis, O.; Kim, Y.; Matsuhisa, N.; Oh, J. Y.; To, J. W.; Mun, J.; Katsumata, T.; Liu, Y.; et al. An integrated self-healable electronic skin system fabricated via dynamic reconstruction of a nanostructured conducting network. *Nat. Nanotechnol.* **2018**, *13*, 1057−1065.

(3) Wang, N.; Yang, X.; Zhang, X. Ultrarobust subzero healable materials enabled by polyphenol nano-assemblies. *Nat. Commun.* **2023**, *14*, 814.

(4) Kim, Y. M.; Kwon, J. H.; Kim, S.; Choi, U. H.; Moon, H. C. Ion-cluster-mediated ultrafast self-healable ionconductors for reconfigurable electronics. *Nat. Commun.* **2022**, *13*, 3769.

(5) Khatib, M.; Zohar, O.; Haick, H. Self-healing soft sensors: from material design to implementation. *Adv. Mater.* **2021**, *33*, 2004190.

(6) Wang, P.; Hu, M.; Wang, H.; Chen, Z.; Feng, Y.; Wang, J.; Ling, W.; Huang, Y. The evolution of flexible electronics: from nature, beyond nature, and to nature. *Adv. Sci.* **2020**, *7*, 2001116.

(7) Ray, T. R.; Choi, J.; Bandodkar, A. J.; Krishnan, S.; Gutruf, P.; Tian, L.; Ghaffari, R.; Rogers, J. A. Bio-integrated wearable systems: a comprehensive review. *Chem. Rev.* **2019**, *119*, 5461−5533.

(8) Choi, S.; Han, S. I.; Kim, D.; Hyeon, T.; Kim, D.-H. High-performance stretchable conductive nanocomposites: materials, processes, and device applications. *Chem. Soc. Rev.* **2019**, *48*, 1566−1595.

(9) Zhang, L. M.; He, Y.; Cheng, S.; Sheng, H.; Dai, K.; Zheng, W. J.; Wang, M. X.; Chen, Z. S.; Chen, Y. M.; Suo, Z. Self-healing,

adhesive, and highly stretchable ionogel as a strain sensor for extremely large deformation. *Small* **2019**, *15*, 1804651.
(10) Zhang, W.; Wu, B.; Sun, S.; Wu, P. Skin-like mechanoresponsive self-healing ionic elastomer from supramolecular zwitterionic network. *Nat. Commun.* **2021**, *12*, 4082.
(11) Liu, C.; Kim, J.-T.; Yang, D. S.; Cho, D.; Yoo, S.; Madhvapathy, S. R.; Jeong, H.; Yang, T.; Luan, H.; Avila, R.; et al. Multifunctional Materials Strategies for Enhanced Safety of Wireless, Skin-Interfaced Bioelectronic Devices. *Adv. Funct. Mater.* **2023**, *33*, 2302256.
(12) Gao, G.; Yang, F.; Zhou, F.; He, J.; Lu, W.; Xiao, P.; Yan, H.; Pan, C.; Chen, T.; Wang, Z. L. Bioinspired Self-Healing Human-Machine Interactive Touch Pad with Pressure-Sensitive Adhesiveness on Targeted Substrates. *Adv. Mater.* **2020**, *32*, 2004290.
(13) Xu, L.; Huang, Z.; Deng, Z.; Du, Z.; Sun, T. L.; Guo, Z. H.; Yue, K. A Transparent, Highly Stretchable, Solvent-Resistant, Recyclable Multifunctional Ionogel with Underwater Self-Healing and Adhesion for Reliable Strain Sensors. *Adv. Mater.* **2021**, *33*, 2105306.
(14) Roels, E.; Terryn, S.; Iida, F.; Bosman, A. W.; Norvez, S.; Clemens, F.; Van Assche, G.; Vanderborght, B.; Brancart, J. Processing of Self-Healing Polymers for Soft Robotics. *Adv. Mater.* **2022**, *34*, 2104798.
(15) Chen, J.; Zhu, Y.; Chang, X.; Pan, D.; Song, G.; Guo, Z.; Naik, N. Recent progress in essential functions of soft electronic skin. *Adv. Funct. Mater.* **2021**, *31*, 2104686.
(16) Zhang, Z.; Ghezawi, N.; Li, B.; Ge, S.; Zhao, S.; Saito, T.; Hun, D.; Cao, P. F. Autonomous self-healing elastomers with unprecedented adhesion force. *Adv. Funct. Mater.* **2021**, *31*, 2006298.
(17) Yang, Y.; Dang, Z. M.; Li, Q.; He, J. Self-healing of electrical damage in polymers. *Adv. Sci.* **2020**, *7*, 2002131.
(18) Markvicka, E. J.; Bartlett, M. D.; Huang, X.; Majidi, C. An autonomously electrically self-healing liquid metal-elastomer composite for robust soft-matter robotics and electronics. *Nat. Mater.* **2018**, *17*, 618−624.
(19) Luo, Y.; Abidian, M. R.; Ahn, J.-H.; Akinwande, D.; Andrews, A. M.; Antonietti, M.; Bao, Z.; Berggren, M.; Berkey, C. A.; Bettinger, C. J.; et al. Technology roadmap for flexible sensors. *ACS Nano* **2023**, *17*, 5211−5295.
(20) Zhang, Q.; Niu, S.; Wang, L.; Lopez, J.; Chen, S.; Cai, Y.; Du, R.; Liu, Y.; Lai, J. C.; Liu, L.; et al. An elastic autonomous self-healing capacitive sensor based on a dynamic dual crosslinked chemical system. *Adv. Mater.* **2018**, *30*, 1801435.
(21) Tan, Y. J.; Susanto, G. J.; Anwar Ali, H. P.; Tee, B. C. Progress and Roadmap for Intelligent Self-Healing Materials in Autonomous Robotics. *Adv. Mater.* **2021**, *33*, 2002800.
(22) Oh, J. Y.; Bao, Z. Second skin enabled by advanced electronics. *Adv. Sci.* **2019**, *6*, 1900186.
(23) Rothemund, P.; Kim, Y.; Heisser, R. H.; Zhao, X.; Shepherd, R. F.; Keplinger, C. Shaping the future of robotics through materials innovation. *Nat. Mater.* **2021**, *20*, 1582−1587.
(24) Cho, S.; Hwang, S. Y.; Oh, D. X.; Park, J. Recent progress in self-healing polymers and hydrogels based on reversible dynamic B-O bonds: boronic/boronate esters, borax, and benzoxaborole. *J. Mater. Chem. A* **2021**, *9*, 14630−14655.
(25) Talebian, S.; Mehrali, M.; Taebnia, N.; Pennisi, C. P.; Kadumudi, F. B.; Foroughi, J.; Hasany, M.; Nikkhah, M.; Akbari, M.; Orive, G.; et al. Self-healing hydrogels: The next paradigm shift in tissue engineering? *Adv. Sci.* **2019**, *6*, 1801664.
(26) Cai, C.; Zhang, X.; Li, Y.; Liu, X.; Wang, S.; Lu, M.; Yan, X.; Deng, L.; Liu, S.; Wang, F.; et al. Self-Healing Hydrogel Embodied with Macrophage-Regulation and Responsive-Gene-Silencing Properties for Synergistic Prevention of Peritendinous Adhesion. *Adv. Mater.* **2022**, *34*, 2106564.
(27) Zhao, X.; Chen, X.; Yuk, H.; Lin, S.; Liu, X.; Parada, G. Soft materials by design: unconventional polymer networks give extreme properties. *Chem. Rev.* **2021**, *121*, 4309−4372.
(28) Wang, S.; Urban, M. W. Self-healing polymers. *Nat. Rev. Mater.* **2020**, *5*, 562−583.
(29) Gu, C.; Wang, M.; Zhang, K.; Li, J.; Lu, Y. L.; Cui, Y.; Zhang, Y.; Liu, C. S. A Full-Device Autonomous Self-Healing Stretchable Soft Battery from Self-Bonded Eutectogels. *Adv. Mater.* **2023**, *35*, 2208392.
(30) Lai, J.-C.; Jia, X.-Y.; Wang, D.-P.; Deng, Y.-B.; Zheng, P.; Li, C.-H.; Zuo, J.-L.; Bao, Z. Thermodynamically stable whilst kinetically labile coordination bonds lead to strong and tough self-healing polymers. *Nat. Commun.* **2019**, *10*, 1164.
(31) Zhao, W.; Zhang, D.; Yang, Y.; Du, C.; Zhang, B. A fast self-healing multifunctional polyvinyl alcohol nano-organic composite hydrogel as a building block for highly sensitive strain/pressure sensors. *J. Mater. Chem. A* **2021**, *9*, 22082−22094.
(32) Zhang, C.; Wang, M.; Jiang, C.; Zhu, P.; Sun, B.; Gao, Q.; Gao, C.; Liu, R. Highly adhesive and self-healing γ-PGA/PEDOT: PSS conductive hydrogels enabled by multiple hydrogen bonding for wearable electronics. *Nano Energy* **2022**, *95*, 106991.
(33) Ratwani, C. R.; Zhao, S.; Huang, Y.; Hadfield, M.; Kamali, A. R.; Abdelkader, A. M. Surface Modification of Transition Metal Dichalcogenide Nanosheets for Intrinsically Self-Healing Hydrogels with Enhanced Mechanical Properties. *Small* **2023**, *19*, 2207081.
(34) Zheng, Y.; Yu, Z.; Zhang, S.; Kong, X.; Michaels, W.; Wang, W.; Chen, G.; Liu, D.; Lai, J.-C.; Prine, N.; et al. A molecular design approach towards elastic and multifunctional polymer electronics. *Nat. Commun.* **2021**, *12*, 5701.
(35) Nian, G.; Kim, J.; Bao, X.; Suo, Z. Making highly elastic and tough hydrogels from doughs. *Adv. Mater.* **2022**, *34*, 2206577.
(36) Shen, Z.; Zhang, Z.; Zhang, N.; Li, J.; Zhou, P.; Hu, F.; Rong, Y.; Lu, B.; Gu, G. High-Stretchability, Ultralow-Hysteresis ConductingPolymer Hydrogel Strain Sensors for Soft Machines. *Adv. Mater.* **2022**, *34*, 2203650.
(37) Meng, X.; Qiao, Y.; Do, C.; Bras, W.; He, C.; Ke, Y.; Russell, T. P.; Qiu, D. Hysteresis-Free Nanoparticle-Reinforced Hydrogels. *Adv. Mater.* **2022**, *34*, 2108243.
(38) Yao, H.; Yang, W.; Cheng, W.; Tan, Y. J.; See, H. H.; Li, S.; Ali, H. P. A.; Lim, B. Z.; Liu, Z.; Tee, B. C. Near-hysteresis-free soft tactile electronic skins for wearables and reliable machine learning. *Proc. Natl. Acad. Sci. U.S.A.* **2020**, *117*, 25352−25359.
(39) Nie, Z.; Kwak, J. W.; Han, M.; Rogers, J. A. Mechanically Active Materials and Devices for Bio-Interfaced Pressure Sensors-A Review. *Adv. Mater.* **2022**, 2205609.
(40) Cai, G.; Wang, J.; Qian, K.; Chen, J.; Li, S.; Lee, P. S. Extremely stretchable strain sensors based on conductive self-healing dynamic cross-links hydrogels for human-motion detection. *Adv. Sci.* **2017**, *4*, 1600190.
(41) Pan, X.; Wang, Q.; He, P.; Liu, K.; Ni, Y.; Chen, L.; Ouyang, X.; Huang, L.; Wang, H.; Xu, S. A bionic tactile plastic hydrogel-based electronic skin constructed by a nerve-like nanonetwork combining stretchable, compliant, and self-healing properties. *Chem. Eng. J.* **2020**, *379*, 122271.
(42) Liao, M.; Wan, P.; Wen, J.; Gong, M.; Wu, X.; Wang, Y.; Shi, R.; Zhang, L. Wearable, healable, and adhesive epidermal sensors assembled from mussel-inspired conductive hybrid hydrogel framework. *Adv. Funct. Mater.* **2017**, *27*, 1703852.
(43) Lu, B.; Lin, F.; Jiang, X.; Cheng, J.; Lu, Q.; Song, J.; Chen, C.; Huang, B. One-pot assembly of microfibrillated cellulose reinforced PVA-borax hydrogels with self-healing and pH-responsive properties. *ACS Sustain. Chem. Eng.* **2017**, *5*, 948−956.
(44) Su, X.; Wang, H.; Tian, Z.; Duan, X.; Chai, Z.; Feng, Y.; Wang, Y.; Fan, Y.; Huang, J. A solvent co-cross-linked organogel with fast self-healing capability and reversible adhesiveness at extreme temperatures. *ACS Appl. Mater. Interfaces* **2020**, *12*, 29757−29766.
(45) Zhang, Y.; Ren, E.; Li, A.; Cui, C.; Guo, R.; Tang, H.; Xiao, H.; Zhou, M.; Qin, W.; Wang, X.; et al. A porous self-healing hydrogel with an island-bridge structure for strain and pressure sensors. *J. Mater. Chem. B* **2021**, *9*, 719−730.
(46) Zhou, X.; Rajeev, A.; Subramanian, A.; Li, Y.; Rossetti, N.; Natale, G.; Lodygensky, G. A.; Cicoira, F. Self-healing, stretchable, and highly adhesive hydrogels for epidermal patch electrodes. *Acta Biomater.* **2022**, *139*, 296−306.

https://doi.org/10.1021/acssensors.3c01835
ACS Sens. XXXX, XXX, XXX−XXX

(47) Liu, S.; Zheng, R.; Chen, S.; Wu, Y.; Liu, H.; Wang, P.; Deng, Z.; Liu, L. A compliant, self-adhesive and self-healing wearable hydrogel as epidermal strain sensor. *J. Mater. Chem. C* **2018**, *6*, 4183−4190.
(48) Redy Keisar, O.; Nahum, V.; Yehezkel, L.; Marcovitch, I.; Columbus, I.; Fridkin, G.; Chen, R. Active and strippable PVA/Borax/NaBO3 hydrogel for effective containment and decontamination of chemical warfare agents. *ACS Omega* **2021**, *6*, 5359−5367.
(49) Paik, J. J.; Jang, B.; Nam, S.; Guo, L. J. A Transparent Poly (Vinyl Alcohol) Ion-Conducting Organohydrogel for Skin-Based Strain-Sensing Applications. *Adv. Healthc. Mater.* **2023**, *12*, 2300076.
(50) Wang, M.; Bai, J.; Shao, K.; Tang, W.; Zhao, X.; Lin, D.; Huang, S.; Chen, C.; Ding, Z.; Ye, J. Poly (vinyl alcohol) hydrogels: The old and new functional materials. *Int. J. Polym. Sci.* **2021**, *2021*, 1−16.
(51) Wang, C.; Shen, Z.; Hu, P.; Wang, T.; Zhang, X.; Liang, L.; Bai, J.; Qiu, L.; Lai, X.; Yang, X.; et al. Facile fabrication and characterization of high-performance Borax-PVA hydrogel. *J. Sol-Gel Sci. Technol.* **2022**, *101*, 103−113.
(52) Alemu, D.; Wei, H.-Y.; Ho, K.-C.; Chu, C.-W. Highly conductive PEDOT: PSS electrode by simple film treatment with methanol for ITO-free polymer solar cells. *Energy Environ. Sci.* **2012**, *5*, 9662−9671.
(53) Hooi, M. T.; Phang, S. W.; Yow, H. Y.; David, E.; Kim, N. X.; Choo, H. L. FTIR spectroscopy characterization and critical comparison of poly (vinyl) alcohol and natural hydroxyapatite derived from fish bone composite for bone-scaffold. *J. Phys.: Conf. Ser.* **2021**, *2120*, 012004.
(54) Li, R.; Wang, L.; Dang, J.; Mi, L.; Han, J.; Mao, M.; Chen, B.; Liu, H. Reconfigurable and tunable photo-controlled hydrogel using hydrogen bonding to drive molecule self-assembly and cross-linking. *J. Mater. Sci.* **2020**, *55*, 14740−14750.
(55) Sun, Y.; Liu, Z.; Zhang, L.; Wang, X.; Li, L. Effects of plasticizer type and concentration on rheological, physico-mechanical and structural properties of chitosan/zein film. *Int. J. Biol. Macromol.* **2020**, *143*, 334−340.
(56) Zheng, H.; Chen, M.; Sun, Y.; Zuo, B. Self-Healing, Wet-Adhesion silk fibroin conductive hydrogel as a wearable strain sensor for underwater applications. *Chem. Eng. J.* **2022**, *446*, 136931.
(57) Liu, H.; Zhang, S.; Li, Z.; Lu, T. J.; Lin, H.; Zhu, Y.; Ahadian, S.; Emaminejad, S.; Dokmeci, M. R.; Xu, F.; et al. Harnessing the wide-range strain sensitivity of bilayered PEDOT: PSS films for wearable health monitoring. *Matter* **2021**, *4*, 2886−2901.
(58) Bhattacharjee, M.; Soni, M.; Escobedo, P.; Dahiya, R. PEDOT: PSS microchannel-based highly sensitive stretchable strain sensor. *Adv. Electron. Mater.* **2020**, *6*, 2000445.
(59) Tang, N.; Zhou, C.; Qu, D.; Fang, Y.; Zheng, Y.; Hu, W.; Jin, K.; Wu, W.; Duan, X.; Haick, H. A highly aligned nanowire-based strain sensor for ultrasensitive monitoring of subtle human motion. *Small* **2020**, *16*, 2001363.
(60) Lam, T. N.; Lee, G. S.; Kim, B.; Dinh Xuan, H.; Kim, D.; Yoo, S. I.; Yoon, J. Microfluidic preparation of highly stretchable natural rubber microfiber containing CNT/PEDOT: PSS hybrid for fabric-sewable wearable strain sensor. *Compos. Sci. Technol.* **2021**, *210*, 108811.
(61) Yuan, J.; Zhang, Y.; Li, G.; Liu, S.; Zhu, R. Printable and stretchable conductive elastomers for monitoring dynamic strain with high fidelity. *Adv. Funct. Mater.* **2022**, *32*, 2204878.
(62) Muth, J. T.; Vogt, D. M.; Truby, R. L.; Mengüç, Y.; Kolesky, D. B.; Wood, R. J.; Lewis, J. A. Embedded 3D printing of strain sensors within highly stretchable elastomers. *Adv. Mater.* **2014**, *26*, 6307−6312.
(63) Lu, Y.; Qu, X.; Zhao, W.; Ren, Y.; Si, W.; Wang, W.; Wang, Q.; Huang, W.; Dong, X. Highly stretchable, elastic, and sensitive MXene-based hydrogel for flexible strain and pressure sensors. *Research* **2020**, *2020*, 2038560.
(64) Chhetry, A.; Sharma, S.; Barman, S. C.; Yoon, H.; Ko, S.; Park, C.; Yoon, S.; Kim, H.; Park, J. Y. Black phosphorus@ laser-engraved graphene heterostructure-based temperature-strain hybridized sensor for electronic-skin applications. *Adv. Funct. Mater.* **2021**, *31*, 2007661.
(65) Li, G.; Huang, K.; Deng, J.; Guo, M.; Cai, M.; Zhang, Y.; Guo, C. F. Highly conducting and stretchable double-network hydrogel for soft bioelectronics. *Adv. Mater.* **2022**, *34*, 2200261.
(66) Liu, Y.-J.; Cao, W.-T.; Ma, M.-G.; Wan, P. Ultrasensitive wearable soft strain sensors of conductive, self-healing, and elastic hydrogels with synergistic "soft and hard" hybrid networks. *ACS Appl. Mater. Interfaces* **2017**, *9*, 25559−25570.
(67) Wang, M.; Chen, Y.; Khan, R.; Liu, H.; Chen, C.; Chen, T.; Zhang, R.; Li, H. A fast self-healing and conductive nanocomposite hydrogel as soft strain sensor. *Colloids Surf., A* **2019**, *567*, 139−149.
(68) Ge, X.; Guo, Y.; Gong, C.; Han, R.; Feng, J.; Ji, J.; Sun, Z.; Gao, J.; Bian, F.; Xu, Z. High Conductivity, Low Impedance, and High Biological Adaptability Ionic Conductive Hydrogels for Ear-Eeg Acquisition. *ACS Appl. Polym. Mater.* **2023**, *5*, 8151−8158.
(69) Lyu, Q.; Gong, S.; Yin, J.; Dyson, J. M.; Cheng, W. Soft wearable healthcare materials and devices. *Adv. Healthc. Mater.* **2021**, *10*, 2100577.
(70) Nittala, A. S.; Karrenbauer, A.; Khan, A.; Kraus, T.; Steimle, J. Computational design and optimization of electro-physiological sensors. *Nat. Commun.* **2021**, *12*, 6351.
(71) de Zea Bermudez, V.; de Almeida, P. P.; Seita, J. F. How to learn and have fun with poly (vinyl alcohol) and white glue. *J. Chem. Educ.* **1998**, *75*, 1410.
(72) Parida, K.; Kumar, V.; Jiangxin, W.; Bhavanasi, V.; Bendi, R.; Lee, P. S. Highly transparent, stretchable, and self-healing ionic-skin triboelectric nanogenerators for energy harvesting and touch applications. *Adv. Mater.* **2017**, *29*, 1702181.
(73) Liu, Y.; Cheng, Y.; Shi, L.; Wang, R.; Sun, J. Breathable, self-adhesive dry electrodes for stable electrophysiological signal monitoring during exercise. *ACS Appl. Mater. Interfaces* **2022**, *14*, 12812−12823.
(74) Ji, Y.; Park, S. M.; Kwon, S.; Leem, J. W.; Nair, V. V.; Tong, Y.; Kim, Y. L. mHealth hyperspectral learning for instantaneous spatiospectral imaging of hemodynamics. *PNAS Nexus* **2023**, *2*, pgad111.
(75) de Melo, G. D.; Lazarini, F.; Levallois, S.; Hautefort, C.; Michel, V.; Larrous, F.; Verillaud, B.; Aparicio, C.; Wagner, S.; Gheusi, G.; et al. COVID-19-related anosmia is associated with viral persistence and inflammation in human olfactory epithelium and brain infection in hamsters. *Sci. Transl. Med.* **2021**, *13*, No. eabf8396.

https://doi.org/10.1021/acssensors.3c01835
ACS Sens. XXXX, XXX, XXX−XXX